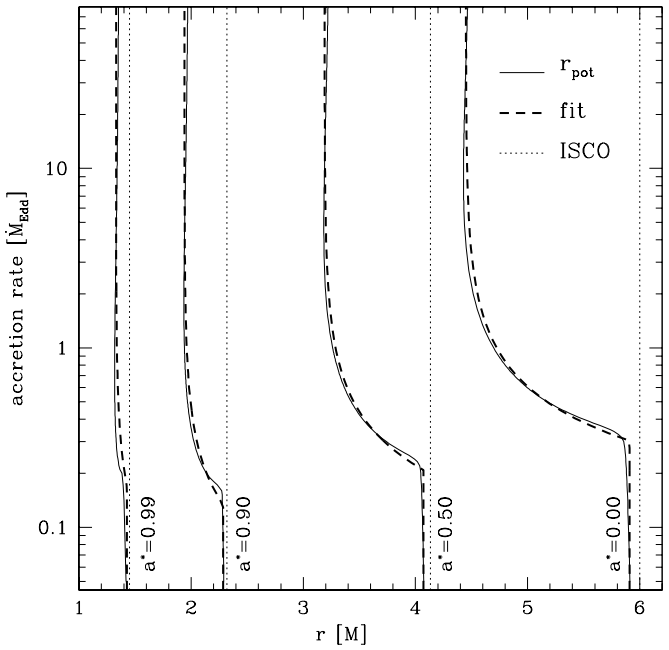

Fig. 6. Location of the potential spout inner edge $r_{\rm pot}$ for viscosity $\alpha = 0.01$ and $a^* = 0$. Solid lines show the exact location of $r_{\rm pot}$ given by equation (1). The approximation (2) is shown by dashed lines, and the location of ISCO by dotted lines.

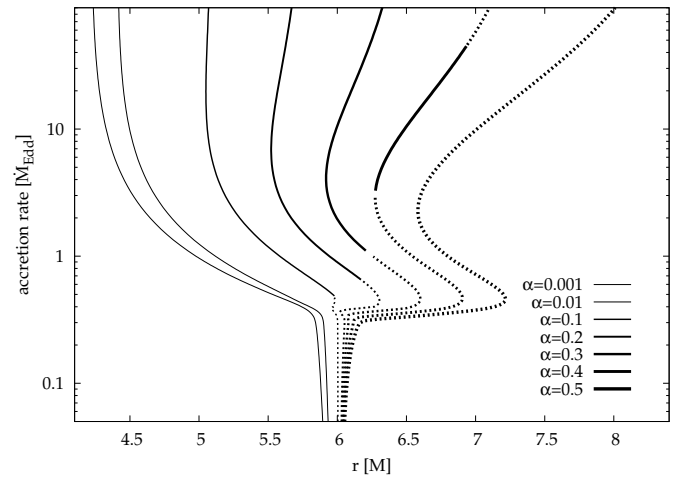

Fig. 7. Location of the sonic point as a function of the accretion rate for different values of α, for a non-rotating black hole, $a^* = 0$. The solid curves are for saddle type solutions while the dotted curves present nodal type regimes.

qualitative change occurs, resembling a "phase transition" from the Shakura-Sunyaev behavior, to a very different slim-disk behavior.

For higher accretion rates the location of the sonic point significantly departs from ISCO. For low values of α the sonic point moves closer to the horizon down to $\sim 4M$ for $\alpha = 0.001$. For $\alpha > 0.2$ the sonic point moves outward with increasing accretion rate reaching values as high as $8M$ for $\alpha = 0.5$ and $100\dot{M}_{\rm Edd}$. This effect was first noticed for small accretion rates by Muchotrzeb-Czerny (1986) and later investigated in a wide range of accretion rates by Abramowicz et al. (1988), who explained it in terms of the disk-Bondi dichotomy. The dependence of the sonic point location on the accretion rate in the near-Eddington regime is more complicated and is related to the fact that in this range of accretion rates the transition from the radiatively efficient disk to the slim disk occurs near the sonic radius.

The topology of the sonic point is important, because physically acceptable solutions must be of the saddle or nodal type; the spiral type is forbidden. The topology may be classified by the eigenvalues $\lambda_1, \lambda_2, \lambda_3$ of the Jacobi matrix,

$$\mathcal{J} = \begin{bmatrix} \frac{\partial \mathcal{D}}{\partial r} & \frac{\partial \mathcal{D}}{\partial \eta} & \frac{\partial \mathcal{D}}{\partial \mathcal{L}} \\ \frac{\partial \mathcal{N}_1}{\partial r} & \frac{\partial \mathcal{N}_1}{\partial \eta} & \frac{\partial \mathcal{N}_1}{\partial \mathcal{L}} \\ \frac{\partial \mathcal{N}_2}{\partial r} & \frac{\partial \mathcal{N}_2}{\partial \eta} & \frac{\partial \mathcal{N}_2}{\partial \mathcal{L}} \end{bmatrix}. \tag{5}$$

Because $\det(\mathcal{J}) = 0$, only two eigenvalues λ_1, λ_2 are non-zero, and the quadratic characteristic equation that determines them takes the form,

$$2\,\lambda^2 - 2\,\lambda\,\mathrm{tr}(\mathcal{J}) - \left[\mathrm{tr}(\mathcal{J}^2) - \mathrm{tr}^2(\mathcal{J})\right] = 0. \tag{6}$$

The nodal type is given by $\lambda_1\lambda_2 > 0$ and the saddle type by $\lambda_1\lambda_2 < 0$, as marked in Figure 7 with the dotted and the solid lines, respectively. For the lowest values of α only the saddle type solutions exist. For moderate values of α ($0.1 \le \alpha \le 0.4$) the topological type of the sonic point changes at least once with increasing accretion rate. For the highest α solutions have only nodal type critical points.

The extra regularity conditions at the sonic point $\mathcal{N}_i(r, \eta, \mathcal{L}) = 0$ are satisfied only for one particular value of the angular momentum at the horizon which is the *eigenvalue* of the problem. $\mathcal{L}_{in}$ is not known a priori, and should be found. Figure 8 shows how does $\mathcal{L}_{in}$ depend on the accretion rate and the α viscosity parameter.

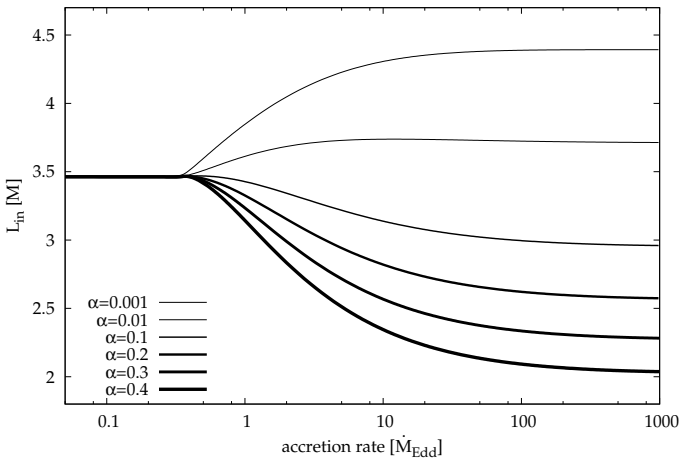

Fig. 8. Angular momentum at the horizon dependence on accretion rate for solutions with different values of α for $a^* = 0$.

5. The variability edge

Axially symmetric and stationary states of slim accretion disks represent, obviously, only a certain theoretical idealization. Real disks are non-axial and non-steady. In particular, one expects transient coherent features at accretion disk surfaces — clumps,